

# Aligned Nanofibers from Polypyrrole/Graphene as Electrodes for Regeneration of Optic Nerve via Electrical Stimulation

Lu Yan,<sup>†</sup> Bingxin Zhao,<sup>†</sup> Xiaohong Liu,<sup>†</sup> Xuan Li,<sup>†</sup> Chao Zeng,<sup>‡</sup> Haiyan Shi,<sup>†</sup> Xiaoxue Xu,<sup>§</sup> Tong Lin,<sup>‡</sup> Liming Dai,<sup>\*,†,||</sup> and Yong Liu<sup>\*,†,⊥</sup>

<sup>†</sup>Lab of Nanoscale Biosensing and Bioimaging, Institute of Advanced Materials for Nano-Bio Applications, School of Ophthalmology & Optometry, Wenzhou Medical University, Wenzhou, Zhejiang 325027, China

<sup>‡</sup>Institute for Frontier Materials, Deakin University, Waurin Ponds, Victoria 3216, Australia

<sup>§</sup>Centre for Biomedical Materials and Engineering, Harbin Engineering University, Harbin, Heilong Jiang 150001, China

<sup>||</sup>Center of Advanced Science and Engineering for Carbon (Case4Carbon), Department of Macromolecular Science and Engineering, Case Western Reserve University, Cleveland, Ohio 44106, United States

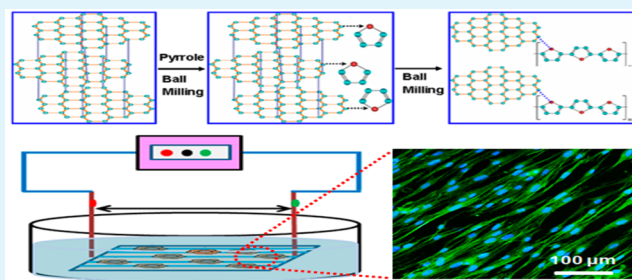
<sup>⊥</sup>Department of Chemistry and Biomolecular Science, Macquarie University, Sydney, New South Wales 2109, Australia

## Supporting Information

**ABSTRACT:** The damage of optic nerve will cause permanent visual field loss and irreversible ocular diseases, such as glaucoma. The damage of optic nerve is mainly derived from the atrophy, apoptosis or death of retinal ganglion cells (RGCs). Though some progress has been achieved on electronic retinal implants that can electrically stimulate undamaged parts of RGCs or retina to transfer signals, stimulated self-repair/regeneration of RGCs has not been realized yet. The key challenge for development of electrically stimulated regeneration of RGCs is the selection of stimulation electrodes with a sufficient safe charge injection limit ( $Q_{inj}$ , i.e., electrochemical capacitance).

Most traditional electrodes tend to have low  $Q_{inj}$  values. Herein, we synthesized polypyrrole functionalized graphene (PPy-G) via a facile but efficient polymerization-enhanced ball milling method for the first time. This technique could not only efficiently introduce electron-acceptor nitrogen to enhance capacitance, but also remain a conductive platform—the  $\pi$ - $\pi$  conjugated carbon plane for charge transportation. PPy-G based aligned nanofibers were subsequently fabricated for guided growth and electrical stimulation (ES) of RGCs. Significantly enhanced viability, neurite outgrowth and antiaging ability of RGCs were observed after ES, suggesting possibilities for regeneration of optic nerve via ES on the suitable nanoelectrodes.

**KEYWORDS:** polypyrrole, N-graphene, nanofibers, retina ganglion cells, electrical stimulation, optical nerve regeneration



## INTRODUCTION

Glaucoma is one of the leading ocular diseases that cause irreversible blindness. It is a kind of permanent optic atrophy and visual field loss due to pathological high intraocular pressure (IOP) and/or retinal ischemia. Typically, high pressure inside the eyes and/or retinal ischemia will cause lesion of retinal ganglion cells (RGCs) and their axons. To date, the general way to deal with glaucoma in clinic therapy is decreasing the IOP by medication or operation. Although the therapy approach can prevent further damage, the lesion of vision functions cannot be recovered. It is known that bioelectricity presented in the human body plays an integral role in maintaining normal biological functions, such as signaling of the nervous system, muscle contraction, and wound healing.<sup>1</sup> One side of the cell is hyperpolarized while the other side is depolarized when the cell was exposed to an electric field,<sup>2</sup> resulted in different fundamental physiological processes across biological membranes.<sup>3,4</sup> Electrical stimulation (ES) has displayed great effects on protection of injured central neurons in vitro<sup>5</sup> and the ability to improve the

survival rates and axon growth of central nervous system in vivo.<sup>6</sup> Optic nerve is composed of RGC axons that flock together at the optic disc and across sclera. Theoretically, it should be possible to regenerate RGC's axons via ES for therapy of glaucoma because glaucoma is generally caused by apoptosis of RGCs. Thus, the use of electrical signals for biomedical applications has attracted great attention. Recent research indicates that the use of ES to enhance RGCs' signal transportation is feasible by using multielectrode arrays (e.g., indium tin oxide and silicon nitride)<sup>7</sup> or nitrogen-doped ultra-nanocrystalline diamond (N-UNCD),<sup>8</sup> though the electrically stimulated regeneration of RGCs is still challenged by the selection of suitable electrodes.

Graphene, a fascinating 2D monolayer of carbon atoms, has recently emerged with many intriguing properties, including electrical conductivity, electrochemical stability, high surface area

Received: December 30, 2015

Accepted: February 29, 2016

Published: February 29, 2016

and biocompatibility.<sup>9</sup> Much attention has been paid in designing graphene based scaffolds for neural regeneration because neural cells are electroactive and functions of nerve systems are related to electrical activities. The large surface area of graphene provides additional advantages for integration of graphene with tissues. However, pure graphene based microelectrodes for ES are hard to achieve due to some drawbacks, including their low  $Q_{inj}$  and poor biocompatibility. To this end, graphene oxide (GO) has been immobilized onto ammonia plasma treated poly(vinyl chloride) nanofibers via electrostatic adhesion, followed by the chemical reduction of GO. The resultant N-doped reduced GO based nanofibers were found to facilitate electrically stimulated growth of spinal motor neuron.<sup>10</sup> Nonconductive biopolymers, such as polylactic acid (PLA) or polylactic-co-glycolic acid (PLGA), have also been hybridized with graphene prepared by chemical vapor deposition, leading to an enhanced differentiation of PC-12 cells with a concomitant reduced conductivity.<sup>11</sup>

In this study, we have incorporated graphene with nitrogen-containing conducting polymers (e.g., polypyrrole) to enhance the capacitance of the electrodes for ES. Conducting polymers (CPs), known as synthetic metals, have been widely investigated for various physiochemical applications. Because CPs possess a conjugated backbone with a high degree of  $\pi$  electron delocalization, they can be readily oxidized or reduced to become either positively charged (oxidative or *p*-doping) or negatively charged (reductive or *n*-doping).<sup>12,13</sup> 3D CP nanofibers can not only provide network substrates for cell adhesion and proliferation but also enhance electron transport for ES.<sup>14</sup> ES via the nanofibrous scaffold could activate the molecular machinery necessary for axon elongation either by inducing nerve action potentials<sup>15</sup> or multicellular healing responses.<sup>16</sup> The 3D nanofibrous structures prepared using electrospinning have been considered as the most suitable scaffolds for ES.<sup>17,18</sup> 3D nanofibrous scaffolds as the biocompatible and electrical conductive substrates for adhesion and proliferation of nerve cells<sup>19</sup> can enlarge the interacting area between the electrode and cells, which is essential for stimulation of nerve cell adhesion and enhanced charge transportation from the electrode to cells.<sup>20</sup> Though 3D CP electrospun nanofibers could be used as substrates for ES, their clinical utilization in tissue engineering is still limited by their poor stability and low conductivity.<sup>21</sup> It is thus essential to introduce more conductive and robust materials, such as graphene into the CP scaffold structure.<sup>22</sup> Particularly, the combination of 3D nanofibrous structures, CPs and graphene can match all properties required for ES.

We have previously demonstrated the synthesis of highly electroactive graphene via edge-functionalized ball milling techniques elsewhere.<sup>23,24</sup> Compared with other traditional techniques for graphene preparation, such as mechanical exfoliation,<sup>9</sup> chemical oxidation<sup>25</sup> and chemical vapor deposition (CVD),<sup>26</sup> the ball milling method is an environmental-friendly, facile, easy to be controlled, and efficient for preparing functionalized graphene with high quality, good structures and properties.<sup>27</sup> In this study, we have prepared CPs (e.g., PPy) functionalized graphene (PPy-G) using a novel polymer polymerization enhanced ball milling (PPEBM) technique. In a typical experiment, PPy was incorporated during the ball milling process to obtain well-defined PPy conjugated graphene hybrids. The as-synthesized PPy-G hybrids with the presence of biocompatible poly(lactic-co-glycolic acid) (PLGA) was subsequently electrospun via a modified electrospinning setup to obtain aligned nanofibrous scaffolds for ES. The resultant aligned nanofibrous scaffold from PPy-G/PLGA was applied as the electrode for the stimulated growth of RGCs.

Dramatically enhanced cell viability, cell length and antiaging ability were obtained after ES. This is consistent with our previously reported preliminary observation that the aligned nanofibers rather than random nanofibers offer additional advantages for stimulation applications for certain specific tissue engineering, including controlled adhesion and oriented growth of nerve cells.<sup>28</sup>

## EXPERIMENTAL SECTION

**Reagents and Materials.** Graphite flakes were provided by Qingdao Haida Corporation. Pyrrole and rhodamine were obtained from Sigma-Aldrich (St. Louis, MO). PLGA was purchased from Lactel Absorbable Polymer company (Birmingham, AL). Dichloromethane (DCM) and *N,N*-dimethylformamide (DMF) were obtained from Aladdin Industrial Corporation (Shanghai, China). The primary RGCs were supplied by Procell company (Wu Han, China). Dulbecco's modified Eagle's medium (DMEM), fetal bovine serum and other cell culture reagents were all obtained from Life Technologies (Carlsbad, CA). Hoechst 33258 for nucleus stain was purchased from Beyotime Biotechnology Institute (Shanghai, China).

**Preparation of Polypyrrole Modified Graphene (PPy-G).** PPy-G was prepared by ball milling of graphite flakes and pyrrole monomer. In a typical process, 10 mg of graphite powder (Qingdao Haida Corporation) and 200  $\mu\text{L}$  of pyrrole (Sigma-Aldrich) were blended in an stainless steel container filled with appropriate size and right amount of stainless steel milling balls (3 mm in diameter, Nanjing NanDa Instrument Plant). The container was then placed in a planetary ball milling machine (Nanjing NanDa Instrument Plant). The samples were vigorously milled at a rate of 500 rpm for 5 h in air at the room temperature. The resulting mixture was subsequently transferred to a 50 mL centrifuge tube containing ethanol. After centrifugation at 2000 rpm for 5 min (to remove large particles), the supernatant was transferred to a dialysis bag (molecular weight cutoff: 8000–14 000, Shanghai Ye'uan biological Ltd.) and soaked in ethanol over 48 h to remove unreacted pyrrole and impurities.

**Fabrication of Nanofibrous Scaffolds.** PLGA (75:25, Lactel Absorbable Polymer) was mixed with PPy-G in DCM/DMF (volume ratio 3:1, Aladdin Industrial Corporation) at various ratios for making electrospinning. The mass ratio of PPy-G to PLGA dispersion was varied from 1:100 to 6:100. A modified electrospinning setup with a high-speed rotating drum as the target collector was used for electrospinning. During electrospinning, the solution was fed at a flow rate in the range of 30–50  $\mu\text{L}/\text{min}$  via a syringe pump. Aligned structured nanofibers were collected on the ITO glass slide mounted on the rotating drum that was covered by the aluminum foil. The applied voltage for electrospinning was controlled at 10–20 kV, and electrospinning distance was 15–20 cm. CCK-8 assay was used to identify the cytotoxicity of PPy-G. (see Supporting Information (SI) for details).

**Electrical Stimulation.** Primary RGCs from SD rats (Procell company) were seeded on the PPy-G/PLGA nanofibers, and then precultured for 24 h. The ES setup is schematically shown in Figure S10. An electrochemical workstation (CHI 760D) was used as a power source. A platinum (Pt) wire contacting with the nanofibers was used as the working electrode. Another Pt wire placed in the cell culture medium was used as the counter electrode. The distance between two Pt electrodes was 1 cm. The ES was conducted by a double pulsed potential chronoamperometry. The forward potential was varied from 0.1 to 1 V/cm while the reverse potential was changed from  $-0.1$  to  $-1$  V/cm. Cells were exposed to the electrical field 1 h each day for 3 days. After treatment, the cells with nanofiber scaffolds were maintained in the incubator at 37 °C with 5% CO<sub>2</sub>. Properties of RGCs were measured after 3 days of culture. For comparison, RGCs on the nanofibers without ES were served as the controls. The neurite length was measured by a microscopy analysis software.

**Confocal Microscopy.** RGCs attached scaffolds were fixed using 4% paraformaldehyde for 20 min, followed by permeabilization of cell membrane with 0.1% Triton-x 100 for 5 min. Rhodamine was subsequently added to stain cytoskeletal for 30 min. The superfluous dyestuff was washed away with PBS. Hoechst 33258 was subsequently

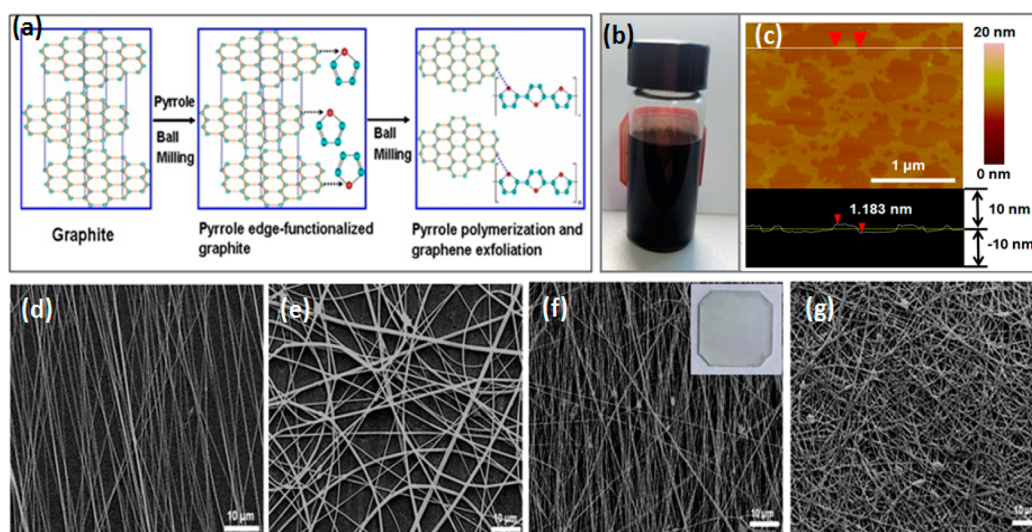


**Figure 1.** (a) Schematic synthesis of the PPy-G via the polymer polymerization enhanced ball milling method. (b) Digital photo of the PPy-G well dispersed in ethanol. (c) AFM micrograph of the PPy-G. (d) SEM micrograph of the aligned nanofibers from 1% (w/w) PPy-G/PLGA dispersion compared to (e) that of the random nanofibers prepared at the identical conditions. (f) SEM micrograph of the aligned nanofibers from 6% (w/w) PPy-G/PLGA dispersion compared to (g) that of the random nanofibers synthesized at the identical conditions. Inset f is the digital photo of the nanofibrous scaffold used for electrical stimulation.

used for nuclear staining, followed by washing with PBS. Cells were imaged using confocal microscopy (Zeiss).

**Cell Aging Study.** RGCs cultured over 10 days were transferred to the 6% PPy-G/PLGA nanofibers. The cells with nanofiber scaffolds were subjected to ES at a pulsed voltage of  $-700$  and  $+700$  mV/cm. RGC cells cultured under the same conditions without ES were used as the control. The ES was performed 1 h each day and continued for 3 days. The resulting cells were subsequently stained green for cytoskeletal, and blue for nuclear. Images of cells were taken using fluorescent microscopy (Olympus).

## RESULTS AND DISCUSSION

Figure 1a schematically shows the synthesis of PPy-G by ball milling graphite and pyrrole. Pyrrole monomer was expected to edge-functionalize graphite sheets via the active nitrogen sites during the initial step. Polymerization of pyrrole occurred as a result of heating during milling friction. As a result of the increase during polymerization, the intersheet distance increased, facilitating the exfoliation of nanosheets. After ball milling, the resulting PPy-G was dispersed well in ethanol as shown in (Figure 1b). No visible aggregation was observed even after the dispersion was left in static condition for 7 days. Morphology and thickness of the as-synthesized PPy-G nanosheets are shown in Figure 1c. The AFM image exhibited that the PPy-G nanosheets distributed uniformly on the substrate. The average thickness was around 1.18 nm.

In this work, biocompatible PLGA was coelectrospun with the PPy-G/ethanol dispersion to improve the spinning ability, and meanwhile enhance the biocompatibility. Randomly oriented nanofibers and aligned nanofibers were fabricated at the same electrospinning condition. The SEM micrographs of as-electrospun nanofibers from both 1% PPy-G (w/w) and 6% PPy-G (w/w) are shown in Figure 1d–g. Well-defined aligned nanofibers with an average diameter around 150 nm were obtained from the dispersion containing 1% PPy-G (Figure 1d), whereas entangled nanofibers with a diameter of 180 nm were obtained when the collector did not rotate during electrospinning (Figure 1e). Aligned fibrous structure was remained well when the content of PPy-G was increased to 6% though the average fiber diameter

decreased by 80 nm (Figure 1c). Typical porous electrospun mats with randomly oriented fibrous structure (around 110 nm) were obtained from 6% PPy-G (Figure 1d). Some fiber beads were visible with increasing amounts of PPy-G, indicating that it was hard to further increase content of PPy-G in the blend fibers. Elemental analysis results indicated that the dominant elements in the PPy-G nanofibers were C, O and N (Figure S1, SI). The element N distributed uniformly along the nanofibers, indicating that the PPy-G evenly blends with PLGA within nanofibers.

The PPy-G and PPy-G/PLGA nanofibers were characterized using various techniques. The corresponding FTIR spectrum of the PPy-G is shown in Figure 2a. Broad bands between 3300 and 3500  $\text{cm}^{-1}$ , arising from N—H stretching vibration, along with the peak at 3000  $\text{cm}^{-1}$  attributable to C—H vibration from the aromatic rings, confirming the presence of PPy in the as-synthesized PPy-G. A very weak band at 2950  $\text{cm}^{-1}$  is associated with the symmetric and asymmetric C—H stretching vibration of saturated hydrocarbons, suggesting the low content of saturated hydrocarbons in the resulting PPy-G. A band at 1650  $\text{cm}^{-1}$  is due to the combined vibration from C=C stretching of graphite base and N—H bending from the PPy base. Two bands at 1540 and 1460  $\text{cm}^{-1}$  are corresponding to C=C stretching in the aromatic rings. The sharp peak at 1050  $\text{cm}^{-1}$  is associated with the vibration of C—N stretching. The alkane (C—H) bend vibration is observed over the range of 500–1000  $\text{cm}^{-1}$ . FTIR results suggest a high percentage content of N and C=C in the as-synthesized PPy-G. These characteristic peaks were all observed in the FTIR spectrum of the PPy-G nanofibers (red curve, Figure 2a), confirming the presence of the PPy-G in the blend nanofibers.

Thermostability of the resulting nanomaterials was determined by thermal gravimetric analysis (TGA). As shown in Figure S2 (SI), the incorporation of PPy-G into PLGA was found to improve the thermostability of nanofibers. PLGA started decomposition at 270 °C whereas the decomposition temperature was increased to 320 °C when PPy-G was presented in PLGA. 10% residual weight remained after complete decomposition of polymers at 350 °C. The observed improved

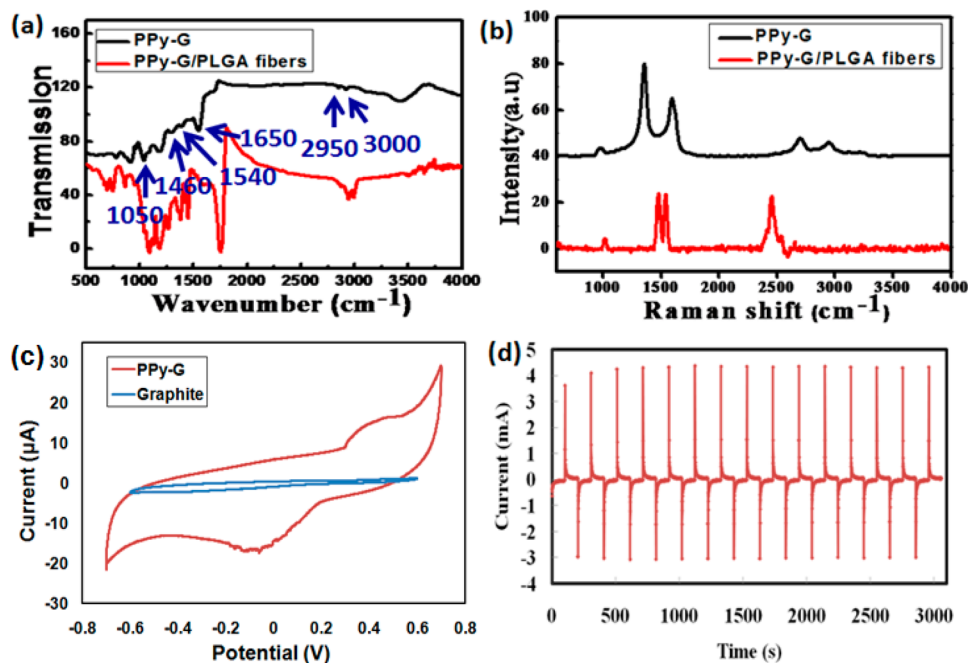


**Figure 2.** (a) FTIR spectra of the PPy-G/PLGA nanofibers compared to the PPy-G. (b) Raman spectra of the PPy-G/PLGA nanofibers compared to the PPy-G. (c) Cyclic voltammograms in 0.1 M PBS solution (pH = 7.4) at the PPy-G and graphite after ball milling without addition of pyrrole for comparison. Electrode size: 1 cm<sup>2</sup>. Scan rate: 50 mV/s. (d) Current–time response (the first 30 steps was shown) during electrical stimulation on the PPy-G/PLGA nanofibers controlled by a double-potential step chronoamperometry. The applied potential steps were +700 and –700 mV/cm vs Ag/AgCl. Pulse width = 0.1 s.

thermostability was attributable to the reduced oxidation by graphene sheets.

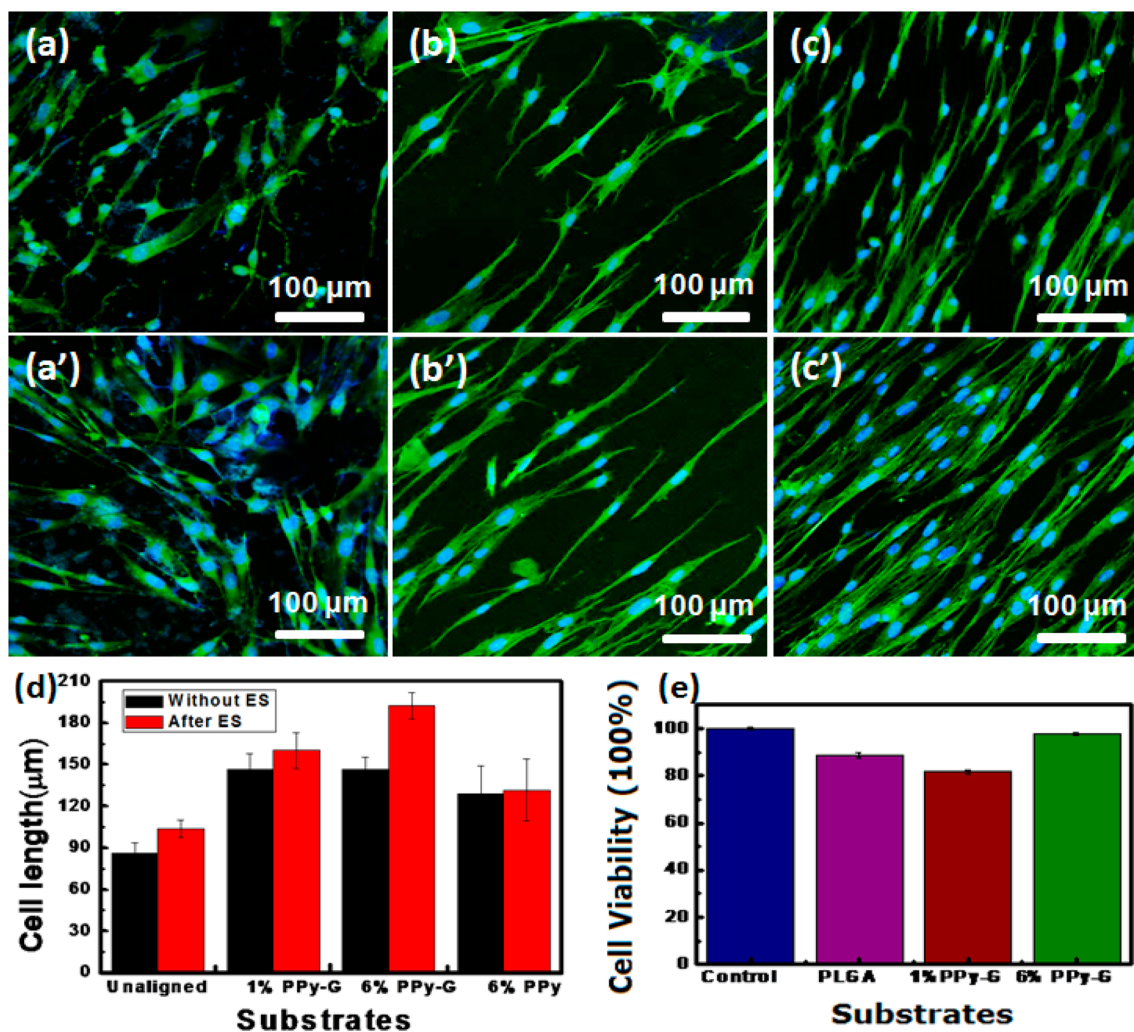
PPy-G in PLGA was further verified by the Raman spectrum. As shown in Figure 2b, the characteristic peak of PPy was visible at 1000 cm<sup>-1</sup>. Three peaks were observed at 1350 cm<sup>-1</sup> (sp<sup>3</sup> carbon, D band), 1580 cm<sup>-1</sup> (sp<sup>2</sup> carbon, G band) and 2700 cm<sup>-1</sup> (2D band) respectively, confirming the presence of graphene structure. The intensity ratio of the D band to G band ( $I_D/I_G$ ) is 1.81, slightly higher than that of the nitrogen-doped graphene prepared using other techniques such as CVD,<sup>24</sup> chemical treatment,<sup>29</sup> microwave,<sup>30</sup> plasma<sup>31</sup> and edge-functionalized ball milling,<sup>27,32</sup> suggesting that the incorporation of PPy caused disorders for graphene. For comparison, the corresponding Raman spectrum of the PPy-G/PLGA nanofibers was also shown in Figure 2b (red curve). One characteristic peaks associated with PPy, and three peaks arisen from D band, G band, and 2D band of graphene were also observed, indicating the existence of PPy-G in the blend nanofibers. Significant shifts at the D band and 2D band were observed for the nanofibers when compared to the pristine PPy-G, presumably due to the interaction between PPy-G and PLGA.

Figure 2c shows the excellent electrochemical activity and capacitance off the resulting PPy-G. One couple of stable redox peaks at +0.47 and –0.08 V (vs Ag/AgCl) due to oxidation and reduction of PPy were evident in the cyclic voltammogram (CV) of PPy-G in 0.1 M phosphate buffer solution (PBS, pH 7.4). For the purpose of comparison, we measured CV at the graphite, which was treated by the same ball milling procedure under identical conditions without addition of pyrrole. There was no significant redox peak presented in the CV of the graphite (blue curve, Figure 2c), confirming that successful polymerization of PPy and the graphene introduced electroactivity to the resulting PPy-G. A much higher CV area was obtained at the PPy-G, indicative of significantly increased surface area arising from

formation of the PPy-G nanosheets. We further measured electrochemical properties of the PPy-G/PLGA aligned nanofibers using CV. The CV result in Figure S4 suggested that much higher peak currents were obtained on the 6% PPy-G/PLGA fiber electrode (blue curve, Figure S4) when compared to that on the 1% PPy-G/PLGA nanofibers (red curve, Figure S4), indicating that higher content of PPy-G in the resulting nanofibers introduced much higher electroactivity, which is beneficial to electrical stimulation. The peak current decreased around 100% when the content of PPy-G in the PLGA nanofibers reduced from 6% to 1%. 6% PPy/PLGA aligned nanofibers without the presence of graphene were further synthesized for comparison. As shown in Figure S4c (green curve), the redox current at the 6% PPy/PLGA nanofibers was negligible when compared to that at the PPy-G/PLGA nanofibers. These results suggested that the presence of graphene in the nanofibers played key roles in determining electroactivity of the resulting electrode.

In vitro growth of RGCs on the PPy-G/PLGA nanofibrous scaffold under periodical electric stimulation was studied. The PPy-G/PLGA nanofibers provided suitable 3D structure with a huge surface area for cell attachment, and their good conductivity offered effective electron transport during ES. A double pulsed potential chronoamperometry was used for ES on the PPy-G/PLGA nanofibers. As shown in Figure 2d, the current decreased gradually at the constant pulsed potential ( $\pm 700$  mV/cm) which prevented RGCs from overpolarization, hence beneficial to the stimulated growth of cell. Figure S5 (SI) shows details on the selection of electrical potential.  $\pm 700$  mV/cm was found to be the best step voltage for ES of RGCs. RGC cells grew well on the random nanofibers as shown in Figure 3a. When the aligned nanofiber network was applied, cell neurites were guided along the fiber (Figure 3b,c).

After electrical stimulation, both cell density and the average length of neurite outgrowth for the RGCs on all substrates



**Figure 3.** Confocal microscopy images of RGC cells seeded on (a) the random PPy-G/PLGA nanofibers without ES and (a') after ES; (b) the aligned PPy-G/PLGA nanofibers with 1% (w/w) PPy-G without ES and (b') after ES; (c) the aligned PPy-G/PLGA nanofibers containing 6% (w/w) PPy-G without ES and (c') after ES. (d) Average cell length of RGCs without and after ES. (e) Cell viability of RGCs cultured on the different substrates. ES conditions: Step potential was pulsed between  $-700$  and  $+700$  mV/cm. ES was performed 1 h everyday and lasted for 3 days.

increased significantly. Cells on the random nanofibers increased by 80 to  $100 \mu\text{m}$  in length when the cells received ES during culture (Figure 3a'). The RGC length became  $140 \mu\text{m}$  and further increased to  $160 \mu\text{m}$  after ES when aligned PPy-G/PLGA nanofibers (PPy-G content 1%) were used (Figure 3b'), confirming that aligned structure could promote the growth of RGCs. When more PPy-G/PLGA, such as 6%, was added to the nanofibers, the cell length increased up to  $190 \mu\text{m}$  (Figure 3c') after ES, whereas the cell length remained  $140 \mu\text{m}$  without ES (Figure 3c). These results suggest that electroactive PPy-G plays key roles in promoting the cell growth under ES. For the purpose of comparison, aligned nanofibers from 6% PPy/PLGA were prepared under the same conditions and used for ES. As shown in Figure S6, aligned nanostructure was useful to guide the outgrowth of RGCs. But change in the cell length after ES was negligible (Figure 3d). This confirmed that the electroactivity of nondoped PPy was too poor to perform ES on RGCs. ES results were in good consent with the CV results. Figure S7 shows SEM images of the cells after ES. Enhanced cell density and length were visible after ES on the random nanofibers (Figure S7a,b). Cell length was further elongated and cell outgrowth was guided very well when the aligned nanofibers were used as the ES electrode (Figure S7c,d).

The cytotoxicity of the as-synthesized PPy-G was evaluated using the CCK-8 assay. All RGC cell viabilities with various amounts of PPy-G (up to  $100 \mu\text{g/mL}$ ) were higher than 90% (Figure S9), suggesting excellent biocompatibility for the resulting PPy-G. The cell viabilities of RGCs on the different ES electrodes were further evaluated. As shown in Figure 3e, all cell viabilities were higher than 80%, indicating good biocompatibility of the as-synthesized PPy-G/PLGA nanofibers. Of particular interest, the cell viability on the 6% PPy-G nanofibers was almost 100% similar to the control, suggesting excellent biocompatibility and the best substrate structure for cell attachment and growth. The cell length sharply increased from  $80 \mu\text{m}$  on the random nanofibers before ES to  $190 \mu\text{m}$  on the aligned nanofibers after ES (Figure 3d). The observed dramatic 137% improvement in cell length suggests that regeneration of RGC is feasible to be realized via ES.

We further studied the effects of ES on antiaging ability of RGCs. RGC cells used in this study were primary RGCs, which are highly differentiated neural cells with a limited lifespan (less than 20 days). Generally, cell viability of the primary RGCs was found to be only 40% after 10 days' culture in vitro due to cell apoptosis or nuclear necrosis.<sup>33</sup> For comparison, the nuclei of RGCs were marked in blue while the cell cytoskeleton was

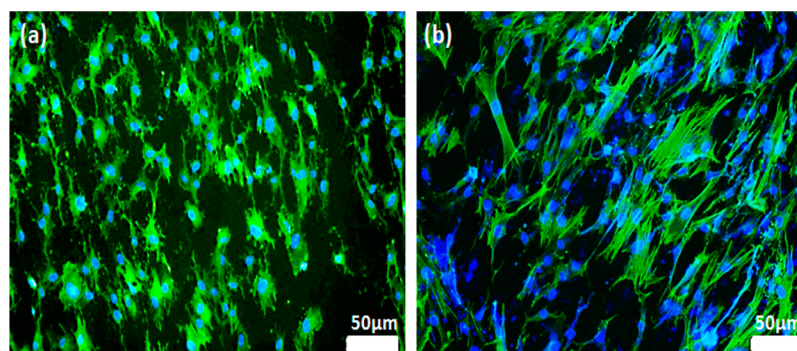


**Figure 4.** Confocal micrographs of aged RGCs on the 6% (w/w) PPy-G/PLGA nanofibers (a) without ES and (b) after ES. All cells were cultured for 10 days. Step potential was pulsed between  $-700$  and  $+700$  mV/cm. ES was performed 1 h everyday and lasted for 3 days.

stained in green. As shown in Figure 4a, RGCs seeded on the PPy-G/PLGA nanofibers without ES showed smaller size, more tentacles, and round in shape after 10 days' culture, suggesting that these cells went through apoptosis and necrosis. RGCs on the nanofibers after ES (Figure 4b), however, remained very good healthy cell morphology. Particularly, the cell length increased from  $50$  to  $107$   $\mu\text{m}$  after ES, indicating that ES enhanced antiaging ability of RGCs.

## CONCLUSIONS

We have synthesized the PPy-G nanosheets by in situ polymerization of pyrrole during ball milling, and PPy-G/PLGA nanofibers using electrospinning. The resulting aligned PPy-G/PLGA nanofibers considerably improved the RGC density and guided the neurite outgrowth of RGCs along the direction of nanofibers. Electrical stimulation led to 137% improvement in cell length with a significantly enhanced antiaging effect for RGCs. Therefore, the aligned nanofibrous scaffold from the PPy-G modified nanocomposites opens up new approaches to the growth of RGCs and regeneration of optical nerve, providing novel alternatives for clinic therapy of optical nerve related diseases, such as glaucoma.

## ASSOCIATED CONTENT

### Supporting Information

The Supporting Information is available free of charge on the ACS Publications website at DOI: 10.1021/acsami.5b12843.

EDS, TGA, CV, selection of the stimulation potential, ES on the 6% PPy/PLGA aligned nanofibers, SEM, immunofluorescence stain, and the schematic ES setup (PDF).

## AUTHOR INFORMATION

### Corresponding Authors

\*L. Dai. Email: liming.dai@case.edu.

\*Y. Liu. Email: yongliu1980@hotmail.com.

### Author Contributions

The paper was written through contributions of all authors. All authors have given approval to the final version of the paper.

### Notes

The authors declare no competing financial interest.

## ACKNOWLEDGMENTS

Authors are grateful to Prof. Ling Hou (Wenzhou Medical University) for providing ARPE-19 cells. Financial supports for this work from National Natural Science Foundation of China

(81301320, 21374081, 51433005, 51201045), Natural Science Foundation of Zhejiang Province (LY13H180013), CWRU-WMU (CON115346), NSF (CMMI-1266295) and MQRDG (9201501614) are acknowledged.

## REFERENCES

- (1) Shi, G.; Zhang, Z.; Rouabhia, M. The Regulation of Cell Functions Electrically using Biodegradable Polypyrrole-poly lactide Conductors. *Biomaterials* **2008**, *29*, 3792–3798.
- (2) Vodovnik, L.; Miklavčič, D.; Serša, G. Modified Cell Proliferation due to Electrical Currents. *Med. Biol. Eng. Comput.* **1992**, *30*, CE21–CE28.
- (3) Du, J.; Feng, L.; Yang, F.; Lu, B. Activity- and  $\text{Ca}^{2+}$ -dependent Modulation of Surface Expression of Brain-derived Neurotrophic Factor Receptors in Hippocampal Neurons. *J. Cell Biol.* **2000**, *150*, 1423–1434.
- (4) Yang, M.; Liang, Y.; Gui, Q.; Chen, J.; Liu, Y. Electroactive Biocompatible Materials for Nerve Cell Stimulation. *Mater. Res. Express* **2015**, *2*, 042001.
- (5) Patel, N.; Poo, M. Orientation of Neurite Growth by Extracellular Electric Fields. *J. Neurosci.* **1982**, *2*, 483–496.
- (6) Morimoto, T.; Fujikado, T.; Choi, J. S.; Kanda, H.; Miyoshi, T.; Fukuda, Y.; Tano, Y. Transcorneal Electrical Stimulation Promotes the Survival of Photoreceptors and Preserves Retinal Function in Royal College of Surgeons Rats. *Invest. Ophthalmol. Visual Sci.* **2007**, *48*, 4725–4732.
- (7) Sekirnjak, C.; Hottoway, P.; Sher, A.; Dabrowski, W.; Litke, A. M.; Chichilnisky, E. J. Electrical Stimulation of Mammalian Retinal Ganglion Cells with Multielectrode Arrays. *J. Neurophysiol.* **2006**, *95*, 3311–3327.
- (8) Hadjinicolaou, A.; Leung, R. T.; Garrett, D. J.; Ganesan, K.; Fox, K.; Nayagam, D. A. X.; Shivdasani, M. N.; Meffin, H.; Ibbotson, M. R.; Praver, S.; O'Brien, B. J. Electrical Stimulation of Retinal Ganglion Cells with Diamond and the Development of an All Diamond Retinal Prosthesis. *Biomaterials* **2012**, *33*, 5812–5820.
- (9) Novoselov, K. S.; Geim, A. K.; Morozov, S. V.; Jiang, D.; Zhang, Y.; Dubonos, S. V.; Grigorieva, I. V.; Firsov, A. A. Electric Field Effect in Atomically Thin Carbon Films. *Science* **2004**, *306*, 666–669.
- (10) Feng, Z.; Wang, T.; Zhao, B.; Li, J.; Jin, L. Soft Graphene Nanofibers Designed for the Acceleration of Nerve Growth and Development. *Adv. Mater.* **2015**, *27*, 6462–6468.
- (11) Sherrell, P. C.; Thompson, B. C.; Wassei, J. K.; Gelmi, A. A.; Higgins, M. J.; Kaner, R. B.; Wallace, G. G. Maintaining Cytocompatibility of Biopolymers Through a Graphene Layer for Electrical Stimulation of Nerve Cells. *Adv. Funct. Mater.* **2014**, *24*, 769–776.
- (12) MacDiarmid, A. G. Nobel Lecture: "Synthetic Metals": a Novel Role for Organic Polymers. *Rev. Mod. Phys.* **2001**, *73*, 701–712.
- (13) Wong, J. Y.; Langer, R.; Ingber, D. E. Electrically Conducting Polymers can Noninvasively Control the Shape and Growth of Mammalian Cells. *Proc. Natl. Acad. Sci. U. S. A.* **1994**, *91*, 3201–3204.
- (14) Ghasemi-Mobarakeh, L.; Prabhakaran, M. P.; Morshed, M.; Nasr-Esfahani, M. H.; Ramakrishna, S. Electrical Stimulation of Nerve Cells

using Conductive Nanofibrous Scaffolds for Nerve Tissue Engineering. *Tissue Eng., Part A* **2009**, *15*, 3605–3619.

(15) Collazos-Castro, J. E.; Muñetón-Gómez, V.; Nieto-Sampedro, M. Olfactory Glia Transplantation into Cervical Spinal Cord Contusion Injuries. *J. Neurosurg.* **2005**, *3*, 308–317.

(16) McCaig, C. D.; Rajnicek, A. M.; Song, B.; Zhao, M. Controlling Cell Behavior Electrically: Current Views and Future Potential. *Physiol. Rev.* **2005**, *85*, 943–978.

(17) Li, M.; Guo, Y.; Wei, Y.; MacDiarmid, A. G.; Lelkes, P. I. Electrospinning Polyaniline-contained Gelatin Nanofibers for Tissue Engineering Applications. *Biomaterials* **2006**, *27*, 2705–2715.

(18) Prabhakaran, M. P.; Ghasemi-Mobarakeh, L.; Jin, G.; Ramakrishna, S. Electrospun Conducting Polymer Nanofibers and Electrical Stimulation of Nerve Stem Cells. *J. Biosci. Bioeng.* **2011**, *112*, 501–507.

(19) Liu, Y.; Gilmore, K.; Chen, J.; Misoska, V.; Wallace, G. G. Bionanowebs Based on Poly(styrene- $\beta$ -isobutylene- $\beta$ -styrene) (SIBS) Containing Single-wall Carbon Nanotubes. *Chem. Mater.* **2007**, *19*, 2721–3723.

(20) Sparreboom, M.; van Schoonhoven, J.; van Zanten, B. G.; Scholten, R. J.; Mylanus, E. A.; Grolman, W.; Maat, A. The Effectiveness of Bilateral Cochlear Implants for Severe-to-profound Deafness in Children: a Systematic Review. *Otology & Neurotology* **2010**, *31*, 1062–1071.

(21) Green, R. A.; Lovell, N. H.; Wallace, G. G.; Poole-Warren, L. A. Conducting Polymers for Neural Interfaces: Challenges in Developing an Effective Long-term Implant. *Biomaterials* **2008**, *29*, 3393–3399.

(22) Tian, H.; Liu, J.; Wei, D.; Kang, X.; Zhang, C.; Du, J.; Yang, B.; Chen, X.; Zhu, H.; Nuli, Y.; Yang, C. S. Graphene Oxide Doped Conducting Polymer Nanocomposite Film for Electrode-tissue Interface. *Biomaterials* **2014**, *35*, 2120–2129.

(23) Yan, L.; Lin, M.; Zeng, C.; Chen, Z.; Zhang, S.; Zhao, X.; Wu, A.; Wang, Y.; Dai, L.; Qu, J.; Guo, M.; Liu, Y. Electroactive and Biocompatible Hydroxyl-functionalized Graphene by Ball Milling. *J. Mater. Chem.* **2012**, *22*, 8367–8371.

(24) Jeon, L.; Sohn, G.-J.; Choi, H.-J.; Bae, S.-Y.; Mahmood, J.; Jung, S.-M.; Seo, J.-M.; Kim, M.-J.; Chang, D.-W.; Dai, L.; Baek, J.-B. Edge-carboxylated Graphene Nanosheets via Ball Milling. *Proc. Natl. Acad. Sci. U. S. A.* **2012**, *109*, 5588–5593.

(25) Li, D.; Müller, M. B.; Gilje, S.; Kaner, R. B.; Wallace, G. G. Processable Aqueous Dispersions of Graphene Nanosheets. *Nat. Nanotechnol.* **2008**, *3*, 101–105.

(26) Qu, L.; Liu, Y.; Baek, J.-B.; Dai, L. Nitrogen-doped Graphene as Efficient Metal-free Electrocatalyst for Oxygen Reduction in Fuel Cells. *ACS Nano* **2010**, *4*, 1321–1326.

(27) Zhang, W.; Li, X.; Zou, R.; Wu, H.; Shi, H.; Yu, S.; Liu, Y. Multifunctional Glucose Biosensors from Fe<sub>3</sub>O<sub>4</sub> Nanoparticles Modified Chitosan/Graphene Nanocomposites. *Sci. Rep.* **2015**, *5*, 11129.

(28) Liu, X.; Chen, J.; Gilmore, K. J.; Higgins, M. J.; Liu, Y.; Wallace, G. G. Guidance of Neurite Outgrowth on Aligned Electrospun Polypyrrole/Poly(styrene- $b$ -isobutylene- $b$ -styrene) Fiber Platforms. *J. Biomed. Mater. Res., Part A* **2010**, *94*, 1004–1011.

(29) Wang, H.; Maiyalagan, T.; Wang, X. Review on Recent Progress in Nitrogen-doped Graphene: Synthesis, Characterization, and Its Potential Applications. *ACS Catal.* **2012**, *2*, 781–794.

(30) Tang, P.; Hu, G.; Gao, Y.; Li, W.; Yao, S.; Liu, Z.; Ma, D. The Microwave Adsorption Behavior and Microwave-assisted Heteroatoms Doping of Graphene-based Nano-carbon Materials. *Sci. Rep.* **2014**, *4*, 5901.

(31) Wang, Y.; Shao, Y.; Matson, D. W.; Li, J.; Lin, Y. Nitrogen-doped Graphene and Its Application in Electrochemical Biosensing. *ACS Nano* **2010**, *4*, 1790–1798.

(32) Jeon, I.-Y.; Choi, H.-J.; Ju, M.-J.; Choi, I.-T.; Lim, K.; Ko, J.; Kim, H.-K.; Kim, J.-J.; Lee, J.-J.; Shin, D.; Jung, S.-M.; Seo, J.-M.; Kim, M.-J.; Park, N.; Dai, L.; Baek, J.-B. Direct Nitrogen Fixation at the Edges of Graphene Nanoplatelets as Efficient Electrocatalysts for Energy Conversion. *Sci. Rep.* **2013**, *3*, 2260.

(33) Zhang, X.; Liu, D. T.; Chiang, S. W.; Choy, K. Y.; Pang, C. P.; Lam, D. S.; Yam, G. H. Immunopanning Purification and Long-term Culture of Human Retinal Ganglion Cells. *Mol. Vis.* **2010**, *16*, 2867–2872.